Advances in Difference Equations
a SpringerOpen Journal

RESEARCH   **Open Access**

CrossMark

An optimized Crank–Nicolson finite difference extrapolating model for the fractional-order parabolic-type sine-Gordon equation

Yanjie Zhou[1] and Zhendong Luo[2*]

*Correspondence: zhdluo@163.com
[2]School of Mathematics and
Physics, North China Electric Power
University, Beijing, China
Full list of author information is
available at the end of the article

Abstract

In this paper, by means of a proper orthogonal decomposition (POD) we mainly reduce the order of the classical Crank–Nicolson finite difference (CCNFD) model for the fractional-order parabolic-type sine-Gordon equations (FOPTSGEs). Toward this end, we will first review the CCNFD model for FOPTSGEs and the theoretical results (such as existence, stabilization, and convergence) of the CCNFD solutions. Then we establish an optimized Crank–Nicolson finite difference extrapolating (OCNFDE) model, including very few unknowns but holding the fully second-order accuracy for FOPTSGEs via POD. Next, by a matrix analysis we will discuss the existence, stabilization, and convergence of the OCNFDE solutions. Finally, we will use a numerical example to validate the validity of theoretical conclusions. Moreover, we show that the OCNFDE model is very valid for settling FOPTSGEs.

MSC: 34K28; 35R11; 65M12

Keywords: Proper orthogonal decomposition; Classical Crank–Nicolson finite difference model; Fractional-order parabolic-type sine-Gordon equation; Optimized Crank–Nicolson finite difference extrapolating model; Existence, stabilization, and convergence

1 Introduction

Though there are lots studies for fractional-order differential equations in recent years (see, e.g., [1–4]), there are few reports about the reduced-order study for the fractional-order differential equations except for Ref. [4]. In this paper, by means of proper orthogonal decomposition (POD) we mainly reduce the order of the classical Crank–Nicolson finite difference (CCNFD) model for the fractional-order parabolic-type sine-Gordon equations (FOPTSGEs) as follows.

$$\frac{\partial \vartheta(t,x)}{\partial t} = K \frac{\partial^\nu \vartheta(t,x)}{\partial |x|^\nu} + \sin(\vartheta(t,x)), \quad (t,x) \in (0,T) \times (0,L), \tag{1}$$

$$\vartheta(t,0) = \vartheta(t,L) = g(t), \quad t \in (0,T), \tag{2}$$

$$\vartheta(0,x) = \varphi(x), \quad x \in (0,L), \tag{3}$$

Springer

where K is the known coefficient of dispersion, $1 < \nu \leq 2$, T is the total time, L is the positive real number, $g(t)$ is a known boundary value function, $\varphi(x)$ is a known initial function, and $\partial^\nu \vartheta(t,x)/\partial|x|^\nu$ is the fractional-order derivative, defined by

$$\frac{\partial^\nu \vartheta(t,x)}{\partial|x|^\nu} = S(\nu)\frac{\partial^2}{\partial x^2}\left(\int_0^x (x-y)^{1-\nu}\vartheta(t,y)\,\mathrm{d}y + \int_x^L (y-x)^{1-\nu}\vartheta(t,y)\,\mathrm{d}y\right), \qquad (4)$$

where $S(\nu) = -[2\cos(\frac{\nu\pi}{2})\Gamma(2-\nu)]^{-1}$ and $\Gamma(\cdot)$ is the Gamma distribution function. For simplicity we further suppose that $g(t) = 0$ in the following discussion.

The FOPTSGEs (1)–(3), which are substantially parabolic-type fraction-order partial differential equations (PDEs) with the nonlinear term $\sin(\vartheta)$, just as the standard fractional-order PDEs in [5–7], also hold very important physical meanings, such as phenomena in fluid dynamics in porous media, groundwater dynamics, and seepage hydraulics groundwater hydraulics (see, e.g., [2, 3, 5, 6]). Nevertheless, the FOPTSGEs (1)–(3) usually have no analytic solution, so that we have to rely on numerical methods (see, e.g., [6, 7]). Recently, a CCNFD model of the FOPTSGEs (1)–(3) has been established in [8], but it contains a lot of unknowns (i.e., degrees of freedom). Therefore, because of the accumulation of the round-off error in the numerical computations, there would appear floating point overflow after a number of computing steps, so that we cannot obtain perfect conclusions. Thus, ensuring that the CCNFD solutions hold the desired accuracy, how to reduce the unknowns of the CCNFD model so as to alleviate the calculated load and the accumulation of the round-off errors in the numerical computations is an urgent problem, which is the main mission in this paper.

POD is regarded as a valid method to reduce the order of numerical models (see [9–12]). It substantially seeks an orthonormal basis from the given data. POD may immensely lessen the unknowns in the numerical formats and has been widely applied in many fields including pattern and signal recognition (see [13]), statistics (see [14]), and hydrodynamics (see [15]). Recently, it has been resoundingly used to the order reduction of the Galerkin, finite element, FD, finite volume element, reduced basis, and meshless methods for PDEs (see, e.g., [16–30]). Nevertheless, the existing most reduced-order models (see, e.g., [9–30]) they are formed with the POD basis produced from the classical numerical solutions at all nodes of time, before repetitively calculating the optimized solutions at the same nodes of time, which are actually some repetitive computations. To eliminate the tautological computations, some optimized FD extrapolating models based on POD have been proposed (see, e.g., [31–34]).

Nevertheless, as far as we know, there has not been any research on the optimized Crank–Nicolson finite difference extrapolating (OCNFDE) scheme of FOPTSGEs constructed by POD. Therefore, in this paper, by POD we build the OCNFDE model only including few unknowns for FOPTSGEs. Specially, we merely choose the CCNFD solutions at the first several nodes of time to form the snapshots, and then use them to produce a set of POD basis, finally use the POD basis to establish the OCNFDE model for finding the OCNFDE solutions at total nodes of time. This is the same thing as utilizing the existing information (on the quite short time interval $[0, T_0]$, $T_0 \ll T$) to forecast the future physical law (on the time interval $[T_0, T]$). Moreover, we will adopt the error estimates to decide the numbers of POD bases. As the OCNFDE model concurrently includes both virtues of POD and the CCNFD model, easily implementing and having the fully second-order accuracy, which is a new development over the reduced-order models in being.

The remaining contents of this paper are arranged as follows. In Sect. 2, we first recall the CCNFD model for the FOPTSGEs (1)–(3) and extract the snapshots from the first few CCNFD solutions. In Sect. 3, we produce a set of POD basis with the snapshots and set up the OCNFDE model. Then, in Sect. 4, by the matrix analysis, we analyze the existence, stabilization, and convergence for the OCNFDE solutions and offer the flowchart of settling the OCNFDE model. Next, in Sect. 5, we use two numerical examples to verify that the conclusions of numerical calculations are accorded with the theory ones. It is also shown that the OCNFDE model is very valid for settling the FOPTSGEs (1)–(3), since it can vastly lessen the number of unknowns, alleviate the calculated load, and save the CPU consumption time and the memory space in the numerical computations. Section 6 finally summarizes the dominating conclusions.

2 The CCNFD model for FOPTSGEs

In this section, we review the CCNFD model for the FOPTSGEs (1)–(3), which has been posed in [8].

Let M and N represent two positive integers, let $h = L/M$ denote the spatial step, and let $\tau = T/N$ denote the time step. The CCNFD model with the fully second-order accuracy for the FOPTSGEs (1)–(3) is denoted as follows:

$$\bar{\vartheta}_i^{n-1} = \vartheta_i^{n-1} + \gamma \left[\sum_{k=0}^{i+1} \omega_k^{(v)} \vartheta_{i-k+1}^{n-1} + \sum_{k=0}^{M-i+1} \omega_k^{(v)} \vartheta_{i+k-1}^{n-1} \right] + \tau \sin\left(\vartheta_i^{n-1}\right), \tag{5}$$

$$\vartheta_i^n = \vartheta_i^{n-1} + \gamma \left[\sum_{k=0}^{i+1} \omega_k^{(v)} \vartheta_{i-k+1}^{n-1} + \sum_{k=0}^{M-i+1} \omega_k^{(v)} \vartheta_{i+k-1}^{n-1} \right] + \frac{\tau}{2} \sin\left(\vartheta_i^{n-1}\right)$$

$$+ \gamma \left[\sum_{k=0}^{i+1} \omega_k^{(v)} \bar{\vartheta}_{i-k+1}^{n-1} + \sum_{k=0}^{M-i+1} \omega_k^{(v)} \bar{\vartheta}_{i+k-1}^{n-1} \right] + \frac{\tau}{2} \sin\left(\bar{\vartheta}_i^{n-1}\right), \tag{6}$$

where $\gamma = -\tau K/[2h^v \cos(v\pi/2)]$, the ϑ_i^n are approximate solutions of $u(t_n, x_i)$ ($i = 1, 2, \ldots, M$), $\omega_0^{(v)} = vg_0^{(v)}/2$, $\omega_k^{(v)} = vg_k^{(v)}/2 + (2 - v)g_{k-1}^{(v)}/2$, $g_0^{(v)} = 1$, $g_k^{(v)} = [1 - (1 + v)/k]g_{k-1}^{(v)}$ ($k = 1, 2, \ldots$).

The sequences $\{\omega_k^{(v)}\}_{k=0}^{\infty}$ and $\{g_k^{(v)}\}_{k=0}^{\infty}$ satisfy the following properties (see, e.g., [3, 35]).

Lemma 1 *As $1 < v \leq 2$, the sequences $\{\omega_k^{(v)}\}_{k=0}^{\infty}$ and $\{g_k^{(v)}\}_{k=0}^{\infty}$ satisfy*

$$g_0^{(v)} = 1, \qquad g_1^{(v)} = -v, \qquad g_2^{(v)} = v(v - 1)/2 > 0,$$

$$1 \geq g_2^{(v)} \geq g_3^{(v)} \geq \cdots \geq 0, \qquad \sum_{k=0}^{\infty} g_k^{(v)} = 0, \qquad \sum_{k=0}^{m} g_k^{(v)} < 0 \quad (m \geq 1);$$

$$\omega_0^{(v)} = v/2, \qquad \omega_1^{(v)} = (2 - v - v^2)/2 < 0, \qquad \omega_2^{(v)} = v(v^2 + v - 4)/4 > 0,$$

$$1 \geq \omega_3^{(v)} \geq \omega_4^{(v)} \geq \cdots \geq 0, \qquad \sum_{k=0}^{\infty} \omega_k^{(v)} = 0, \qquad \sum_{k=0}^{m} \omega_k^{(v)} < 0 \quad (m \geq 2).$$

Put

$$\boldsymbol{B} = \begin{bmatrix} \omega_1^{(v)} & \omega_0^{(v)} & 0 & \cdots & 0 & 0 \\ \omega_2^{(v)} & \omega_1^{(v)} & \omega_0^{(v)} & \cdots & 0 & 0 \\ \omega_3^{(v)} & \omega_2^{(v)} & \omega_1^{(v)} & \cdots & 0 & 0 \\ \vdots & \vdots & \vdots & \ddots & \vdots & \vdots \\ \omega_{M-2}^{(v)} & \omega_{M-3}^{(v)} & \omega_{M-4}^{(v)} & \cdots & \omega_1^{(v)} & \omega_0^{(v)} \\ \omega_{M-1}^{(v)} & \omega_{M-2}^{(v)} & \omega_{M-3}^{(v)} & \cdots & \omega_2^{(v)} & \omega_1^{(v)} \end{bmatrix}, \qquad \boldsymbol{G}(\boldsymbol{V}^{n-1}) = \begin{bmatrix} \sin(\vartheta_1^{n-1}) \\ \sin(\vartheta_2^{n-1}) \\ \sin(\vartheta_3^{n-1}) \\ \vdots \\ \sin(\vartheta_{M-2}^{n-1}) \\ \sin(\vartheta_{M-1}^{n-1}) \end{bmatrix},$$

$$\boldsymbol{V}^n = \left[\vartheta_1^n, \vartheta_2^n, \ldots, \vartheta_{M-2}^n, \vartheta_{M-1}^n \right]^T, \qquad \bar{\boldsymbol{V}}^n = \left[\bar{\vartheta}_1^n, \bar{\vartheta}_2^n, \ldots, \bar{\vartheta}_{M-2}^n, \bar{\vartheta}_{M-1}^n \right]^T,$$

$$\boldsymbol{E} = -\gamma \left[\boldsymbol{B} + \boldsymbol{B}^T \right].$$

Therefore, the CCNFD model (5)–(6) can be presented in the following matrix format:

$$\bar{\boldsymbol{V}}^{n-1} = \boldsymbol{V}^{n-1} + \boldsymbol{E}\boldsymbol{V}^{n-1} + \tau \boldsymbol{G}(\boldsymbol{V}^{n-1}), \tag{7}$$

$$\boldsymbol{V}^n = \boldsymbol{V}^{n-1} + \frac{1}{2}\boldsymbol{E}(\boldsymbol{V}^{n-1} + \bar{\boldsymbol{V}}^{n-1}) + \frac{\tau}{2}\left[\boldsymbol{G}(\boldsymbol{V}^{n-1}) + \boldsymbol{G}(\bar{\boldsymbol{V}}^{n-1}) \right]. \tag{8}$$

Furthermore, the vector-format CCNFD model (7)–(8) can be reduced as follows:

$$\boldsymbol{V}^n = \boldsymbol{V}^{n-1} + \frac{1}{2}\boldsymbol{E}\big(2\boldsymbol{V}^{n-1} + \boldsymbol{E}\boldsymbol{V}^{n-1} + \tau \boldsymbol{G}(\boldsymbol{V}^{n-1})\big)$$

$$+ \frac{\tau}{2}\big[\boldsymbol{G}(\boldsymbol{V}^{n-1}) + \boldsymbol{G}(\boldsymbol{V}^{n-1} + \boldsymbol{E}\boldsymbol{V}^{n-1} + \tau \boldsymbol{G}(\boldsymbol{V}^{n-1}))\big], \quad n = 1, 2, \ldots, N, \tag{9}$$

satisfying the following initial values:

$$\boldsymbol{V}^0 = \left[\vartheta_1^0, \vartheta_2^0, \ldots, \vartheta_{M-2}^0, \vartheta_{M-1}^0 \right]^T, \quad \vartheta_i^0 = \varphi(0, ih), i = 1, 2, \ldots, M-1. \tag{10}$$

Apparently, there is a unique set of the solution vector $\{\boldsymbol{V}^n\}_{n=1}^N$ for the vector-format CCNFD model (9). The following stabilization and convergence of the set of the solution $\{\boldsymbol{V}^n\}_{n=1}^N$ has been proved in [35, Theorem 2].

Theorem 2 *As $\|\boldsymbol{I} + \boldsymbol{E}\|_\infty \leq 1$, the set of solution $\{\boldsymbol{V}^n\}_{n=1}^N$ for the CCNFD model (9) is stable and convergent. Furthermore, the error estimates between the set of solution $\{\boldsymbol{V}^n\}_{n=1}^N$ for the CCNFD model (9) and $\tilde{\boldsymbol{V}}(t_n) = [\vartheta(t_n, x_1), \vartheta(t_n, x_2), \ldots, \vartheta(t_n, x_{M-1})]^T$ $(n = 1, 2, \ldots, N)$ produced from the analytic solution of the FOPTSGEs (1)–(3) are denoted by*

$$\left\| \tilde{\boldsymbol{V}}(t_n) - \boldsymbol{V}^n \right\|_\infty = O(\tau^2, h^2), \quad n = 1, 2, \ldots, N, \tag{11}$$

the above $\boldsymbol{I}$ is the unit matrix, $\|\tilde{\boldsymbol{B}}\|_\infty = \max_{1 \leq i \leq m} \sum_{j=1}^m |a_{i,j}|$ (for any matrix $\tilde{\boldsymbol{B}} = (a_{i,j})_{m \times m}$), and $\|\boldsymbol{V}^i\|_\infty = \max_{1 \leq j \leq M-1} |\vartheta_j^i|$ (for any $\boldsymbol{V}^i = (\vartheta_1^i, \vartheta_2^i, \ldots, \vartheta_{M-1}^i)^T \in \mathbb{R}^{M-1}$).

Remark 3 We easily see from Lemma 1 that the assumption $\|\boldsymbol{I} + \boldsymbol{E}\|_\infty \leq 1$ is reasonable. Therefore, as long as we provide the spatial step h, the time step τ, the coefficient K, the initial value φ, and parameters v, by settling the vector-format CCNFD model (9) we can obtain the set of the solution $\{\boldsymbol{V}^n\}_{n=1}^N$. We extract the first l solution vectors $\boldsymbol{V}^1, \boldsymbol{V}^2, \ldots, \boldsymbol{V}^l$

($l \ll N$) in the set of solution $\{\boldsymbol{V}^n\}_{n=1}^{N}$ for the CCNFD model (9) as a group of snapshots.

3 The OCNFDE model for FOPTSGEs

3.1 Production and results of POD basis

To the snapshots $\boldsymbol{V}^1, \boldsymbol{V}^2, \ldots, \boldsymbol{V}^l$ ($l \ll N$) obtained in Sect. 2, let $\boldsymbol{B}_\vartheta = (\boldsymbol{V}^1, \boldsymbol{V}^2, \ldots, \boldsymbol{V}^l)$ (apparently $\boldsymbol{B}_\vartheta \in \mathbb{R}^{(M-1) \times l}$), let $\lambda_j > 0$ ($j = 1, 2, \ldots, r =: \operatorname{rank}(\boldsymbol{B}_\vartheta)$) be the positive eigenvalues of $\boldsymbol{B}_\vartheta \boldsymbol{B}_\vartheta^T$ arranged nonincreasingly, and let $\boldsymbol{V}_\vartheta = (\boldsymbol{\phi}_1, \boldsymbol{\phi}_2, \ldots, \boldsymbol{\phi}_r) \in \mathbb{R}^{(M-1) \times r}$ be the orthonormal eigenvectors of $\boldsymbol{B}_\vartheta \boldsymbol{B}_\vartheta^T$ associated with the positive eigenvalues. Thus, a set of POD basis $\boldsymbol{\Psi} =: (\boldsymbol{\phi}_1, \boldsymbol{\phi}_2, \ldots, \boldsymbol{\phi}_d)$ ($d \le r$) is obtained from the initial d eigenvectors in $\boldsymbol{V}_\vartheta$ and holds the following result (see, e.g., [20, 21, 36]):

$$\left\| \boldsymbol{B}_\vartheta - \boldsymbol{\Psi} \boldsymbol{\Psi}^T \boldsymbol{B}_\vartheta \right\|_{2,2} = \sqrt{\lambda_{d+1}}, \tag{12}$$

where $\|\boldsymbol{B}_\vartheta\|_{2,2} = \sup_{\boldsymbol{x} \in \mathbb{R}^{M-1}} \|\boldsymbol{B}_\vartheta \boldsymbol{x}\|_2 / \|\boldsymbol{x}\|_2$, and $\|\boldsymbol{x}\|_2$ is the l^2 norm for the vector $\boldsymbol{x} \in \mathbb{R}^{M-1}$. Furthermore, we have

$$\begin{aligned}
\left\| \boldsymbol{V}^n - \boldsymbol{\Psi} \boldsymbol{\Psi}^T \boldsymbol{V}^n \right\|_2 &= \left\| \left(\boldsymbol{B}_\vartheta - \boldsymbol{\Psi} \boldsymbol{\Psi}^T \boldsymbol{B}_\vartheta \right) \boldsymbol{\varepsilon}^n \right\|_2 \\
&\le \left\| \boldsymbol{B}_\vartheta - \boldsymbol{\Psi} \boldsymbol{\Psi}^T \boldsymbol{B}_\vartheta \right\|_{2,2} \left\| \boldsymbol{\varepsilon}^n \right\|_2 \\
&\le \sqrt{\lambda_{d+1}}, \quad n = 1, 2, \ldots, l,
\end{aligned} \tag{13}$$

where $\boldsymbol{\varepsilon}_n$ ($n = 1, 2, \ldots, l$) represent a set of unit orthogonal vectors with nth component being 1. Thus, $\boldsymbol{\Psi} = (\boldsymbol{\phi}_1, \boldsymbol{\phi}_2, \ldots, \boldsymbol{\phi}_d)$ forms a set of POD basis.

Remark 4 Because the order l of the matrix $\boldsymbol{A}_\vartheta^T \boldsymbol{A}_\vartheta$ is far smaller than the order $M-1$ of the matrix $\boldsymbol{A}_\vartheta \boldsymbol{A}_\vartheta^T$, that is, the number of the snapshots l is far smaller than that of the spatial internal nodes $M-1$, whereas both positive eigenvalues λ_i ($i = 1, 2, \ldots, r$) are the same, we may first find the eigenvectors $\boldsymbol{\psi}_i$ and the eigenvalues λ_i ($i = 1, 2, \ldots, r$) of $\boldsymbol{A}_\vartheta^T \boldsymbol{A}_\vartheta$, and then compute the eigenvectors $\boldsymbol{\varphi}_i$ of $\boldsymbol{A}_\vartheta \boldsymbol{A}_\vartheta^T$ via the formula $\boldsymbol{\varphi}_i = \boldsymbol{A}_\vartheta \boldsymbol{\psi}_i / \sqrt{\lambda_i}$ ($i = 1, 2, \ldots, r$), so that the POD basis can be obtained expediently.

3.2 The OCNFDE model of the FOPTSGEs

From Sect. 3.1 we have obtained the first l OCNFDE solutions $\boldsymbol{V}_d^n = \boldsymbol{\Psi} \boldsymbol{\Psi}^T \boldsymbol{V}^n =: \boldsymbol{\Psi} \boldsymbol{\beta}_d^n$ ($n = 1, 2, \ldots, l \le N$), where $\boldsymbol{V}_d^n = (u_{d,1}^n, u_{d,2}^n, \ldots, u_{d,M-2}^n, u_{d,M-1}^n)^T$ and $\boldsymbol{\beta}_d^n = (\beta_1^n, \beta_2^n, \ldots, \beta_d^n)^T$. At the moment, replacing $\boldsymbol{V}^n$ in (9) with $\boldsymbol{V}_d^n = \boldsymbol{\Psi} \boldsymbol{\beta}_d^n$ ($n = l+1, l+2, \ldots, N$), we can obtain the following OCNFDE model:

$$\begin{cases}
\boldsymbol{\Psi} \boldsymbol{\beta}_d^n = \boldsymbol{\Psi} \boldsymbol{\Psi}^T \boldsymbol{V}^n, & n = 1, 2, \ldots, l; \\
\boldsymbol{\Psi} \boldsymbol{\beta}_d^n = \boldsymbol{\Psi} \boldsymbol{\beta}_d^{n-1} + \frac{1}{2} \boldsymbol{E}(2 \boldsymbol{\Psi} \boldsymbol{\beta}_d^{n-1} + \boldsymbol{E} \boldsymbol{\Psi} \boldsymbol{\beta}_d^{n-1} + \tau \boldsymbol{G}(\boldsymbol{\Psi} \boldsymbol{\beta}_d^{n-1})) & \\
\quad + \frac{\tau}{2} [\boldsymbol{G}(\boldsymbol{\Psi} \boldsymbol{\beta}_d^{n-1}) + \boldsymbol{G}(\boldsymbol{\Psi} \boldsymbol{\beta}_d^{n-1} + \boldsymbol{E} \boldsymbol{\Psi} \boldsymbol{\beta}_d^{n-1} + \tau \boldsymbol{G}(\boldsymbol{\Psi} \boldsymbol{\beta}_d^{n-1}))], & l+1 \le n \le N, \\
\boldsymbol{V}_d^n = \boldsymbol{\Psi} \boldsymbol{\beta}_d^n, & n = 1, 2, \ldots, N,
\end{cases} \tag{14}$$

where $\boldsymbol{V}^n$ ($n = 1, 2, \ldots, l$) are the given CCNFD solution vectors for the CCNFD model (9). The OCNFDE model (14) is reduced to the following model:

$$
\begin{cases}
\boldsymbol{\beta}_d^n = \boldsymbol{\Psi}_\vartheta^T \boldsymbol{V}^n, & 1 \le n \le l; \\
\boldsymbol{\beta}_d^n = \boldsymbol{\beta}_d^{n-1} + \frac{1}{2} \boldsymbol{\Psi}^T \boldsymbol{E} [2 \boldsymbol{\Psi} \boldsymbol{\beta}_d^{n-1} + \boldsymbol{E} \boldsymbol{\Psi} \boldsymbol{\beta}_d^{n-1} + \tau \boldsymbol{G}(\boldsymbol{\Psi} \boldsymbol{\beta}_d^{n-1})] \\
\qquad + \frac{\tau}{2} \boldsymbol{\Psi}^T [\boldsymbol{G}(\boldsymbol{\Psi} \boldsymbol{\beta}_d^{n-1}) + \boldsymbol{G}(\boldsymbol{\Psi} \boldsymbol{\beta}_d^{n-1} + \boldsymbol{E} \boldsymbol{\Psi} \boldsymbol{\beta}_d^{n-1} + \tau \boldsymbol{G}(\boldsymbol{\Psi} \boldsymbol{\beta}_d^{n-1}))], & l+1 \le n \le N, \\
\boldsymbol{V}_d^n = \boldsymbol{\Psi} \boldsymbol{\beta}_d^n, & 1 \le n \le N.
\end{cases}
\tag{15}
$$

Remark 5 Since the CCNFD model (9) includes ($M - 1$) unknowns at each node of time, but the OCNFDE model (15) at the same node of time has only d unknowns ($d \ll M - 1$), the OCNFDE model (15) is far superior to the CCNFD model (9).

4 The existence, stabilization, and convergence for the OCNFDE solutions and the flowchart for settling the OCNFDE model

4.1 The existence, stabilization, and convergence for the OCNFDE solutions
Apparently, there is a unique set of the solution vector $\{\boldsymbol{V}_d^n\}_{n=1}^N$ for the OCNFDE model (15). Further, the stabilization and convergence for the OCNFDE solutions have the following result.

Theorem 6 *Under the same conditions of Theorem* 2, *the series of solutions* $\{\boldsymbol{V}_d^n\}_{n=1}^N$ *of the OCNFDE model* (15) *is stable and convergent and has the following error estimates*:

$$
\left\| \boldsymbol{V}^n - \boldsymbol{V}_d^n \right\|_\infty \le \rho(n) \sqrt{\lambda_{d+1}}, \quad n = 1, 2, \ldots, N,
\tag{16}
$$

the above $\boldsymbol{V}^i$ ($i = 1, 2, \ldots, N$) *represents the CCNFD solution vectors of the CCNFD model* (9), $\rho(n) = 1$ ($1 \le n \le l$), *and* $\rho(n) = (1 + 2\tau + \tau^2)^{n-l}$ ($l + 1 \le n \le N$). *Furthermore, we have the error estimates between the analytic solution vectors* $\tilde{\boldsymbol{V}}(t_n) = [u(t_n, x_1), u(t_n, x_2), \ldots, u(t_n, x_{M-1})]^T$ ($n = 1, 2, \ldots, N$) *of the FOPTSGEs* (1)–(3) *and the OCNFDE solutions* $\boldsymbol{V}_d^n$ *of the OCNFDE model* (15) *as follows*:

$$
\left\| \tilde{\boldsymbol{V}}^n - \boldsymbol{V}_d^n \right\|_\infty \le C \left[\tau^2 + h^2 + \rho(n) \sqrt{\lambda_{d+1}} \right], \quad n = 1, 2, \ldots, N,
\tag{17}
$$

where C is a generic positive constant.

Proof (1) *The stabilization and convergence of the OCNFDE solutions*
   By $\boldsymbol{V}_d^n = \boldsymbol{\Psi} \boldsymbol{\beta}_d^n$ ($n = 1, 2, \ldots, N$) we can restore the OCNFDE model (14) as follows:

$$
\boldsymbol{V}_d^n = \boldsymbol{\Psi} \boldsymbol{\Psi}^T \boldsymbol{V}^n, \quad 1 \le n \le l;
\tag{18}
$$

$$
\boldsymbol{V}_d^n = \boldsymbol{V}_d^{n-1} + \frac{1}{2} \boldsymbol{E} \left(2 \boldsymbol{V}_d^{n-1} + \boldsymbol{E} \boldsymbol{V}_d^{n-1} + \tau \boldsymbol{G}(\boldsymbol{V}_d^{n-1}) \right)
$$
$$
+ \frac{\tau}{2} \left[\boldsymbol{G}(\boldsymbol{V}_d^{n-1}) + \boldsymbol{G}(\boldsymbol{V}_d^{n-1} + \boldsymbol{E} \boldsymbol{V}_d^{n-1} + \tau \boldsymbol{G}(\boldsymbol{V}_d^{n-1})) \right], \quad l+1 \le n \le N.
\tag{19}
$$

As the CCNFD solutions $\boldsymbol{V}^n$ ($n = 1, 2, \ldots, l$) are given and stable, the stabilization of $\boldsymbol{V}_d^n$ ($n = 1, 2, \ldots, l$) can obtained by $\boldsymbol{V}_d^n = \boldsymbol{\Psi} \boldsymbol{\Psi}^T \boldsymbol{V}^n$ ($n = 1, 2, \ldots, l$) of (18) and $\|\boldsymbol{V}_d^n\|_\infty \le \|\boldsymbol{V}^n\|_\infty$ ($n = 1, 2, \ldots, l$).

As $\|I + E\|_\infty \leq 1$, we obtain

$$
\begin{aligned}
\left\| I + E + \frac{1}{2}E^2 \right\|_\infty &= \left\| \frac{1}{2}\big[I + (I + E)^2 \big] \right\|_\infty \\
&\leq \frac{1}{2}\big(1 + \|I + E\|_\infty \big) \\
&\leq 1.
\end{aligned}
\tag{20}
$$

Using the differential mean value theorem, we have

$$
\big\| G\big(V(t_i)\big) - G\big(V^i\big) \big\|_\infty \leq \big\| V(t_i) - V^i \big\|_\infty,
\tag{21}
$$

$$
\big\| G\big(V^i\big) \big\|_\infty \leq \big\| V^i \big\|_\infty.
\tag{22}
$$

Hence, by (20)–(22) from (9) we have

$$
\begin{aligned}
\big\| V_d^n \big\|_\infty &\leq \left\| V_d^{n-1} + \frac{1}{2}E\big(2V_d^{n-1} + EV_d^{n-1} \big) \right\|_\infty + \left\| \frac{\tau}{2}EG\big(V_d^{n-1}\big) \right\|_\infty \\
&\quad + \left\| \frac{\tau}{2}\big[G\big(V_d^{n-1}\big) + G\big(V_d^{n-1} + EV_d^{n-1} + \tau G\big(V_d^{n-1}\big)\big) \big] \right\|_\infty \\
&\leq \left\| I + E + \frac{1}{2}E^2 \right\|_\infty \big\| V_d^{n-1} \big\|_\infty + \frac{\tau}{2}\|E\|_\infty \big\| G\big(V_d^{n-1}\big) \big\|_\infty \\
&\quad + \frac{\tau}{2}\big[\big\| G\big(V_d^{n-1}\big) \big\|_\infty + \big\| G\big(V_d^{n-1} + EV_d^{n-1} + \tau G\big(V_d^{n-1}\big)\big) \big\|_\infty \big] \\
&\leq \big\| V_d^{n-1} \big\|_\infty + \frac{\tau}{2}\|E\|_\infty \big\| V_d^{n-1} \big\|_\infty + \frac{\tau}{2}\big\| V_d^{n-1} \big\|_\infty \\
&\quad + \frac{\tau}{2}\big\| (I + E)V_d^{n-1} + \tau G\big(V_d^{n-1}\big) \big\|_\infty \\
&\leq \big\| V_d^{n-1} \big\|_\infty + \frac{\tau}{2}\|E\|_\infty \big\| V_d^{n-1} \big\|_\infty + \tau \big\| V_d^{n-1} \big\|_\infty + \frac{\tau^2}{2}\big\| V_d^{n-1} \big\|_\infty \\
&= (1 + \beta\tau)\big\| V_d^{n-1} \big\|_\infty, \quad n = l+1, l+2, \ldots, N,
\end{aligned}
\tag{23}
$$

where $\beta = \tau/2 + 1 + \|E\|_\infty/2$. Because $\|E\|_\infty = \| -I + I + E \|_\infty \leq \|I\|_\infty + \|I + E\|_\infty \leq 2$, we have $\beta \leq \tau/2 + 2 \leq \tau + 2$. Thus, by iterating (23) and from Theorem 2 and $\|V_d^n\|_\infty \leq \|V^n\|_\infty$ ($n = 1, 2, \ldots, l$) we have

$$
\begin{aligned}
\big\| V_d^n \big\|_\infty &\leq (1 + \beta\tau)^{n-l} \big\| V_d^l \big\|_\infty \\
&\leq (1 + \beta\tau)^n \big\| V^0 \big\|_\infty \\
&\leq \big\| V^0 \big\|_\infty \exp\big[(2 + \tau)n\tau \big] \\
&\leq \big\| V^0 \big\|_\infty \exp\big[(2 + \tau)T \big], \quad n = l+1, l+2, \ldots, N,
\end{aligned}
\tag{24}
$$

which shows that the OCNFDE solutions $\{V_d^n\}_{n=l+1}^N$ are stable and convergent according to the Lax stabilization theorem (see [10]). Therefore, the solutions $\{V_d^n\}_{n=1}^N$ for the OCNFDE model (15) is stable. Moreover, by Lax's stabilization theorem (see. e.g., [37, 38]) we deduce that the OCNFDE solutions $\{V_d^n\}_{n=1}^N$ are convergent.

(2) *The error estimates* (11) *of the CCNFD solutions* $\{\boldsymbol{V}_d^n\}_{n=1}^N$

As $n = 1, 2, \ldots, l$, by the properties of norm and (13) we straight-away obtain the error estimations:

$$\left\| \boldsymbol{V}^n - \boldsymbol{V}_d^n \right\|_\infty \leq \left\| \boldsymbol{V}^n - \boldsymbol{V}_d^n \right\|_2 = \left\| \boldsymbol{V}^n - \boldsymbol{\Psi} \boldsymbol{\Psi}^T \boldsymbol{V}^n \right\|_2 \leq \sqrt{\lambda_{d+1}}, \quad 1 \leq n \leq l. \tag{25}$$

Let $\boldsymbol{e}_n = \boldsymbol{V}^n - \boldsymbol{V}_d^n$. By subtracting (19) from (9) we get

$$\begin{aligned}
\boldsymbol{e}_n &= \boldsymbol{e}_{n-1} + \frac{1}{2}\boldsymbol{E}\left(2\boldsymbol{e}_{n-1} + \boldsymbol{E}\boldsymbol{e}_{n-1} + \tau\boldsymbol{G}\left(\boldsymbol{V}^{n-1}\right) - \tau\boldsymbol{G}\left(\boldsymbol{V}_d^{n-1}\right)\right) \\
&\quad + \frac{\tau}{2}\left[\boldsymbol{G}\left(\boldsymbol{V}^{n-1}\right) + \boldsymbol{G}\left(\boldsymbol{V}^{n-1} + \boldsymbol{E}\boldsymbol{V}^{n-1} + \tau\boldsymbol{G}\left(\boldsymbol{V}^{n-1}\right)\right)\right. \\
&\quad \left. - \boldsymbol{G}\left(\boldsymbol{V}_d^{n-1}\right) - \boldsymbol{G}\left(\boldsymbol{V}_d^{n-1} + \boldsymbol{E}\boldsymbol{V}_d^{n-1} + \tau\boldsymbol{G}\left(\boldsymbol{V}_d^{n-1}\right)\right)\right] \\
&= \frac{\tau}{2}\left[\boldsymbol{G}\left(\boldsymbol{V}^{n-1} + \boldsymbol{E}\boldsymbol{V}^{n-1} + \tau\boldsymbol{G}\left(\boldsymbol{V}^{n-1}\right)\right)\right. \\
&\quad \left. - \boldsymbol{G}\left(\boldsymbol{V}_d^{n-1} + \boldsymbol{E}\boldsymbol{V}_d^{n-1} + \tau\boldsymbol{G}\left(\boldsymbol{V}_d^{n-1}\right)\right)\right] + \left(\boldsymbol{I} + \boldsymbol{E} + \frac{1}{2}\boldsymbol{E}^2\right)\boldsymbol{e}_{n-1} \\
&\quad + \frac{\tau}{2}(\boldsymbol{I} + \boldsymbol{E})\left[\boldsymbol{G}\left(\boldsymbol{V}^{n-1}\right) - \boldsymbol{G}\left(\boldsymbol{V}_d^{n-1}\right)\right], \quad l+1 \leq n \leq N.
\end{aligned} \tag{26}$$

Thus, by (20)–(22), from (26), we have

$$\begin{aligned}
\|\boldsymbol{e}_n\|_\infty &\leq \left\| \boldsymbol{I} + \boldsymbol{E} + \frac{1}{2}\boldsymbol{E}^2 \right\|_\infty \|\boldsymbol{e}_{n-1}\|_\infty + \frac{\tau}{2}\|\boldsymbol{E}\|_\infty \|\boldsymbol{e}_{n-1}\|_\infty \\
&\quad + \frac{\tau}{2}\left[\|\boldsymbol{e}_{n-1}\|_\infty + \|\boldsymbol{I} + \boldsymbol{E}\|_\infty \|\boldsymbol{e}_{n-1}\|_\infty + \tau\|\boldsymbol{e}_{n-1}\|_\infty\right] \\
&\leq (1 + \beta\tau)\|\boldsymbol{e}_{n-1}\|_\infty \\
&\leq \left(1 + 2\tau + \tau^2\right)\|\boldsymbol{e}_{n-1}\|_\infty, \quad n = l+1, l+2, \ldots, N.
\end{aligned} \tag{27}$$

Thus, by iterating (27), and using (25), we have

$$\begin{aligned}
\|\boldsymbol{e}_n\|_\infty &\leq \left(1 + 2\tau + \tau^2\right)^{n-l}\|\boldsymbol{e}_l\|_\infty \\
&\leq \left(1 + 2\tau + \tau^2\right)^{n-l}\sqrt{\lambda_{d+1}}, \quad n = l+1, l+2, \ldots, N.
\end{aligned} \tag{28}$$

Combining (25) with (28) yields (16), and combining Theorem 2 with (16) yields (17). This finishes the proof of Theorem 6. □

Remark 7 The error terms $\sqrt{\lambda_{d+1}}$ and $\rho(n) = (1 + 2\tau + \tau^2)^{n-l}$ $(l+1 \leq n \leq N)$ in Theorem 6 are generated by the order reduction of the CCNFD model (9) and the extrapolating iteration, respectively. They can, respectively, act as the judgment for choosing the number d of POD bases and updating the POD basis in the numerical calculations. Although the OCNFDE solutions slightly reduce little accuracy in comparison with the CCNFD ones, they can immensely reduce the unknowns so that they can greatly lessen the accumulation of the round-off error and enhance calculative efficiency, as stated in the numerical example in Sect. 5. However, the lots numerical experiments base on POD have proven that the eigenvalues λ_j $(j = 1, 2, \ldots, l)$ of the matrix $\boldsymbol{B}_\vartheta \boldsymbol{B}_\vartheta^T$ are generally decreasing quickly

to zero. Thus, if we select d that satisfies $(1 + 2\tau + \tau^2)^{N-l}\sqrt{\lambda_{d+1}} \leq \min\{\tau^2, h^2\}$, then we can ensure that the OCNFDE solutions reach the optimal convergence order, i.e., when we select d that satisfies $(1 + 2\tau + \tau^2)^{N-l}\sqrt{\lambda_{d+1}} \leq \min\{\tau^2, h^2\}$, the OCNFDE solutions have second-order accuracy.

4.2 Flowchart of settling the OCNFDE model
The flowchart for settling the ROESTCFE model of the FOPTSGEs (1)–(3) consists of the following six steps.

Step 1 Extract the snapshots $\boldsymbol{V}^i$ ($i = 1, 2, \ldots, l$, usually $l = 20$) from the first l CCNFD solutions of the CCNFD model:

$$\boldsymbol{V}^n = \boldsymbol{V}^{n-1} + \frac{1}{2}\boldsymbol{E}\big(2\boldsymbol{V}^{n-1} + \boldsymbol{E}\boldsymbol{V}^{n-1} + \tau\boldsymbol{G}\big(\boldsymbol{V}^{n-1}\big)\big)$$
$$+ \frac{\tau}{2}\big[\boldsymbol{G}\big(\boldsymbol{V}^{n-1}\big) + \boldsymbol{G}\big(\boldsymbol{V}^{n-1} + \boldsymbol{E}\boldsymbol{V}^{n-1} + \tau\boldsymbol{G}\big(\boldsymbol{V}^{n-1}\big)\big)\big], \quad n = 1, 2, \ldots, l,$$

satisfying the following initial value conditions:

$$\boldsymbol{V}^0 = \big[\vartheta_1^0, \vartheta_2^0, \ldots, \vartheta_{M-2}^0, \vartheta_{M-1}^0\big]^T, \quad \vartheta_i^0 = \varphi(0, ih), i = 1, 2, \ldots, M - 1.$$

Step 2 Form the snapshot matrix $\boldsymbol{A}_\vartheta = [\boldsymbol{V}^1, \boldsymbol{V}^2, \ldots, \boldsymbol{V}^l]$.

Step 3 Compute the eigenvalues $\lambda_1 \geq \lambda_2 \geq \cdots \geq \lambda_r > 0$ and the corresponding eigenvectors $\boldsymbol{\psi}^j$ ($j = 1, 2, \ldots, r =: \dim\{\boldsymbol{V}^1, \boldsymbol{V}^2, \ldots, \boldsymbol{V}^l\}$) of the matrix $\boldsymbol{A}_\vartheta^T \boldsymbol{A}_\vartheta$.

Step 4 For the given time step τ and spatial step h and the desired error bound $\delta = O(\tau^2, h^2)$, choose the number d of the POD basis that satisfies $\lambda_{d+1} \leq \delta^2$.

Step 5 Formulate the POD basis $\boldsymbol{\Psi} = [\boldsymbol{\varphi}_1, \boldsymbol{\varphi}_2, \ldots, \boldsymbol{\varphi}_d]$ by $\boldsymbol{\varphi}_i = \boldsymbol{A}_\vartheta \boldsymbol{\psi}_i / \sqrt{\lambda_i}$ ($i = 1, 2, \ldots, d$) and obtain the OCNFDE solutions by settling the OCNFDE model:

$$\begin{cases} \boldsymbol{\beta}_d^n = \boldsymbol{\Psi}_\vartheta^T \boldsymbol{V}^n, & 1 \leq n \leq l; \\ \boldsymbol{\beta}_d^n = \boldsymbol{\beta}_d^{n-1} + \frac{1}{2}\boldsymbol{\Psi}^T \boldsymbol{E}(2\boldsymbol{\Psi}\boldsymbol{\beta}_d^{n-1} + \boldsymbol{E}\boldsymbol{\Psi}\boldsymbol{\beta}_d^{n-1} + \tau\boldsymbol{G}(\boldsymbol{\Psi}\boldsymbol{\beta}_d^{n-1})) & \\ \quad + \frac{\tau}{2}\boldsymbol{\Psi}^T[\boldsymbol{G}(\boldsymbol{\Psi}\boldsymbol{\beta}_d^{n-1}) + \boldsymbol{G}(\boldsymbol{\Psi}\boldsymbol{\beta}_d^{n-1} + \boldsymbol{E}\boldsymbol{\Psi}\boldsymbol{\beta}_d^{n-1} + \tau\boldsymbol{G}(\boldsymbol{\Psi}\boldsymbol{\beta}_d^{n-1}))], & l + 1 \leq n \leq N, \\ \boldsymbol{V}_d^n = \boldsymbol{\Psi}\boldsymbol{\beta}_d^n, & 1 \leq n \leq N, \end{cases}$$

which only contains d unknowns.

Step 6 On condition that $(1 + 2\tau + \tau^2)^{n-l}\sqrt{\lambda_{d+1}} = O(\tau^2, h^2)$ ($n = l + 1, l + 2, \ldots, N$), then end; else, let $\boldsymbol{V}^i = \boldsymbol{V}_d^{n-l-i}$ ($i = 1, 2, \ldots, l$), then return to Step 2.

5 Two numerical examples
In this following, we offer two numerical examples to explain that the advantage of the OCNFDE model (15) of the FOPTSGEs (1)–(3).
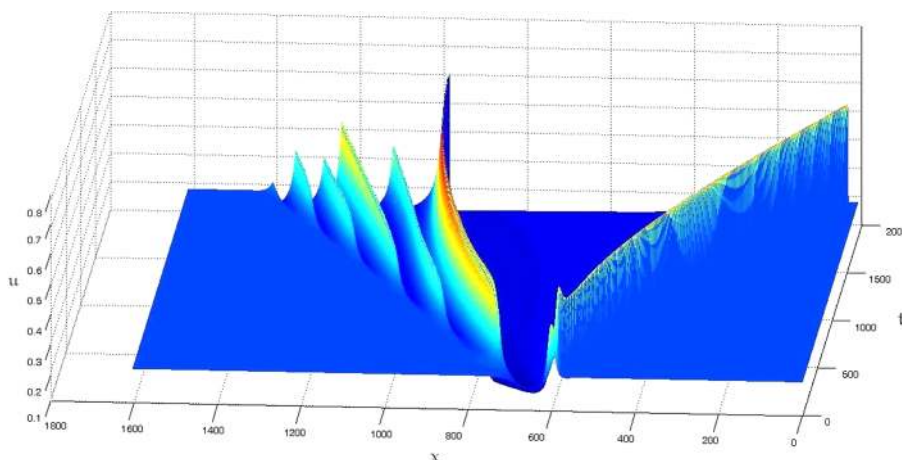
5.1 The comparison between the OCNFDE and CCNFD solutions
In the FOPTSGEs (1)–(3), we choose $T = 2000$ (i.e., $0 \leq t \leq 2000$), $L = 16{,}000$ (i.e., $0 \leq x \leq 16{,}000$), $\tau = h = 0.01$, $K = 1$, $v = 1.5$, the boundary value $g(t) = 0.22$, and the initial function

$$u(0, x) = \varphi(x) = \begin{cases} 0.22 + \sin(\pi x/2000), & x \in [6000, 8000], \\ 0.22, & x \in [0, 6000] \cup [8000, 16{,}000]. \end{cases}$$

Under this case, it is not easy to seek the analytical solution of the FOPTSGEs (1)–(3), so that we have to rely on the numerical solutions.

We first find the first $l = 20$ solution vectors $\boldsymbol{V}^n$ ($n = 1, 2, \ldots, 20$) by the CCNFD model (9) and form the snapshot matrix $\boldsymbol{B}_\vartheta = [\boldsymbol{V}^1, \boldsymbol{V}^2, \ldots, \boldsymbol{V}^{20}]$. Then by Steps 3 and 5 in Sect. 4.2 we find the eigenvalues $\lambda_1 \geq \lambda_2 \geq \cdots \geq \lambda_{20} \geq 0$ and the corresponding eigenvectors $\boldsymbol{\varphi}_j$ ($j = 1, 2, \ldots, 20$). By estimating we gain that $\sqrt{\lambda_7} \leq 3.5 \times 10^{-4}$. Thus, we choose the POD basis $\boldsymbol{\Psi} = [\boldsymbol{\varphi}_1, \boldsymbol{\varphi}_2, \ldots, \boldsymbol{\varphi}_6]$ and compute the OCNFDE solutions ϑ_{di}^n ($n = 1, 2, \ldots, 200{,}000$ and $i = 1, 2, \ldots, 1{,}600{,}000$, i.e., $0 < t \leq 2000$ and $0 \leq x \leq 16{,}000$) via the OCNFDE model (15), and depict them graphically in Fig. 1. To compare with the OCNFDE solutions, we also find the CCNFD solutions ϑ_i^n ($n = 1, 2, \ldots, 200{,}000$ and $i = 1, 2, \ldots, 1{,}600{,}000$, i.e., $0 < t \leq 2000$ and $0 \leq x \leq 16{,}000$) via the CCNFD model (9), and depict them graphically in Fig. 2. Although Fig. 2 and Fig. 1 are almost the same, by carefully comparing we find that the conclusions of the OCNFDE solutions in Fig. 1 are better than those of the CCNFD solutions in Fig. 2.

Figure 1 The ROENBE solutions when $0 \leq t \leq 2000$ and $0 \leq x \leq 16{,}000$
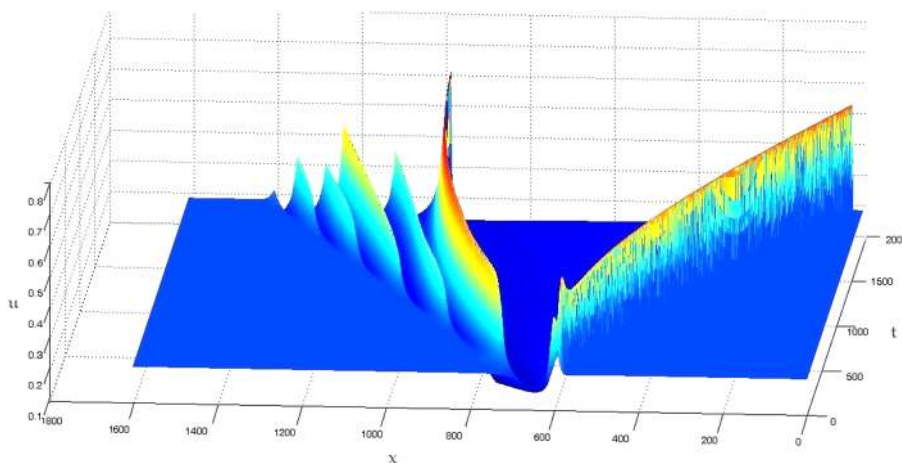
Figure 2 The CCNFD solutions when $0 \leq t \leq 2000$ and $0 \leq x \leq 16{,}000$
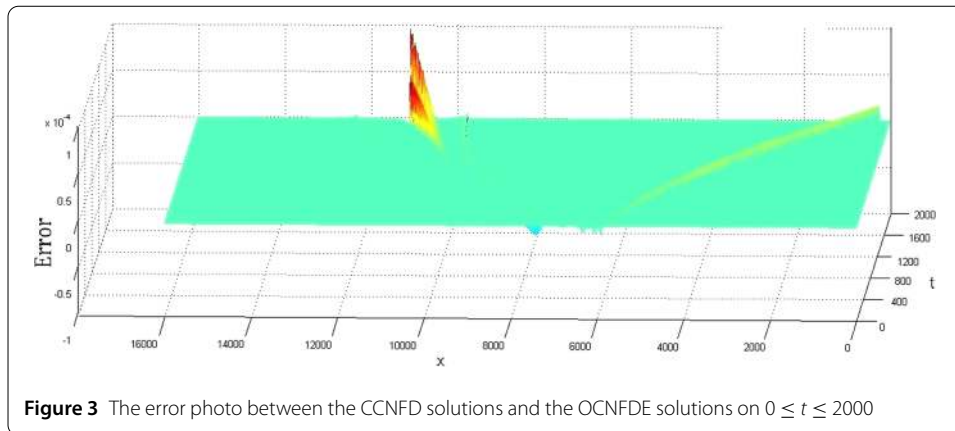
Figure 3 The error photo between the CCNFD solutions and the OCNFDE solutions on $0 \le t \le 2000$

Table 1 Comparisons of errors and CPU time of the CCNFD and OCNFDE solutions

Real time	CCNFD scheme		OCNFDE scheme	
	Error $\|\tilde{\boldsymbol{V}}(t_n) - \boldsymbol{V}^n\|_2$	CPU time	Error $\|\tilde{\boldsymbol{V}}(t_n) - \boldsymbol{V}_d^n\|_2$	CPU time
$n = 100{,}000$	0.00046	381 s	0.00048	3.0 s
$n = 150{,}000$	0.00058	571 s	0.00063	4.5 s
$n = 200{,}000$	0.00076	762 s	0.00082	6.0 s

Figure 3 shows the error photo between the CCNFD solutions and the OCNFDE solutions on $0 \le t \le 2000$, which accords with the theoretical conclusion of (16) in Theorem 6, since both the theoretical and the numerical errors are $O(10^{-4})$ as $\tau = h = 0.01$.

As the CCNFD model at each node of time includes 1,600,000 unknowns, but the OCNFDE model at the same node of time only contains six unknowns, the OCNFDE model can immensely alleviate the accumulation of the round-off error in the numerical computation and enhance the accuracy of the OCNFDE numerical solutions. From the records for settling the CCNFD model and the OCNFDE model in the same Laptop (iPone Mac book: Int Core i5 Processor, 16 GB RAM) we find that the CPU consumption time for settling the CCNFD model on $0 \le t \le 2000$ is 762 min, whereas the CPU consumption time for settling the OCNFDE model is less than 6 min, that is, the CPU consumption time for settling the CCNFD model is 126 times more than that for settling the OCNFDE model. More comparisons of errors and CPU time of the CCNFD and OCNFDE solutions are listed in Table 1, where $\|\tilde{\boldsymbol{V}}(t_n) - \boldsymbol{V}^n\|_2$ and $\|\tilde{\boldsymbol{V}}(t_n) - \boldsymbol{V}_d^n\|_2$ are approximately estimated by $\|\boldsymbol{V}^{n+1} - \boldsymbol{V}^n\|_2$ and $\|\boldsymbol{V}_d^{n+1} - \boldsymbol{V}_d^n\|_2$, respectively.

Table 1 further shows that the numerical computing conclusions accord with the theoretical ones. This implies that the OCNFDE model is effective for settling the FOPTSGEs (1)–(3) and that the OCNFDE model is far superior to the CCNFD model.

5.2 The comparison between the OCNFDE method and OCNFDE/DEI method

When we solve the OCNFDE model (15), we need to compute the following nonlinear terms:

$$\boldsymbol{G}^{\mathrm{POD}}\left(\beta_d^{n-1}\right) =: \boldsymbol{\Psi}^T \boldsymbol{G}\left(\boldsymbol{\Psi}\beta_d^{n-1}\right),$$

which includes some complex computations depending on the number of unknowns $M - 1$, since $\boldsymbol{\Psi}\beta_d^{n-1}$ has $M - 1$ rows. In order to reduce further the computational load

for solving the OCNFDE model ([15](#)), we adopt a discrete-empirical-interpolation (EDI) method for the nonlinear terms $\boldsymbol{G}(\boldsymbol{\Psi}\boldsymbol{\beta}_d^{n-1})$, i.e., the nonlinear terms $\boldsymbol{G}(\boldsymbol{\Psi}\boldsymbol{\beta}_d^{n-1})$ are approximated with the EDI terms $\boldsymbol{G}^{\mathrm{EDI}}$ as follows:

$$\boldsymbol{G}^{\mathrm{POD}}\big(\beta_d^{n-1}\big) \simeq \boldsymbol{G}^{\mathrm{EDI}}\big(\beta_d^{n-1}\big) =: \boldsymbol{\Psi}^T\hat{\boldsymbol{G}}\big(\boldsymbol{P}^T\hat{\boldsymbol{G}}\big)^{-1}P^T\boldsymbol{G}\big(\boldsymbol{\Psi}\boldsymbol{\beta}_d^{n-1}\big),$$

where $\hat{\boldsymbol{G}} \in \mathbb{R}^{(M-1)\times d}$ contains the first d POD bases produced by the snapshots $\boldsymbol{G}(\boldsymbol{V}^n)$ ($n = 1, 2, \ldots, L$) associated with the largest d eigenvalues, $\boldsymbol{P} = [\boldsymbol{e}_{\rho_1}, \boldsymbol{e}_{\rho_2}, \ldots, \boldsymbol{e}_{\rho_d}] \in \mathbb{R}^{(M-1)\times d}$ consists of the rows of $\boldsymbol{G}$ corresponding to the DEIM indices $\rho_1, \rho_2, \ldots, \rho_d$ that are obtained by the greedy algorithm (see [29, 39]).

In the second example, we choose $T = 2.5$ (i.e., $0 \leq t \leq 2.5$), $L = 2.7$ (i.e., $0 \leq x \leq 2.5$), $\tau = h = 0.01$, $K = 1$, $\nu = 1.5$, the boundary value $g(t) = x(2.5 - x)\sin(0.8\pi x)\exp(-t)$, and the initial function $u(0, x) = \varphi(x) = x(2.5 - x)\sin(0.8\pi x)$.

Similarly, we first find the first $l = 20$ solution vectors $\boldsymbol{V}^n$ ($n = 1, 2, \ldots, 20$) by the CCNFD model ([9](#)) and form the snapshot matrix $\boldsymbol{B}_\vartheta = [\boldsymbol{V}^1, \boldsymbol{V}^2, \ldots, \boldsymbol{V}^{20}]$. Then by Steps 3 and 5 in Sect. [4.2](#) we find the eigenvalues $\lambda_1 \geq \lambda_2 \geq \cdots \geq \lambda_{20} \geq 0$ and the corresponding eigenvectors $\boldsymbol{\varphi}_j$ ($j = 1, 2, \ldots, 20$). By estimating we achieve that $\sqrt{\lambda_6} \leq 2.4 \times 10^{-4}$, which implies that we only need to choose the POD basis $\boldsymbol{\Psi} = [\boldsymbol{\varphi}_1, \boldsymbol{\varphi}_2, \ldots, \boldsymbol{\varphi}_5]$ and compute the OCNFDE and OCNFDE/EDI solutions ϑ_{di}^n and $\vartheta_{\mathrm{EDI}i}^n$ ($n = 1, 2, \ldots, 250$ and $i = 1, 2, \ldots, 250$, i.e., $0 < t \leq 2.5$ and $0 \leq x \leq 2.5$) via the OCNFDE model ([15](#)) and the OCNFDE/EDI model (whose $\boldsymbol{G}$ in ([15](#)) is replaced with $\boldsymbol{G}^{\mathrm{EDI}}$), and depict them graphically in Figs. [4](#) and [5](#), respectively. Figures [4](#) and [5](#) are almost the same.

To quantify the efficiency of the OCNFDE and OCNFDE/DEI methods, we compare the CPU time between the OCNFDE and OCNFDE/DEI methods, the root mean square errors (RMSE) between the CCNFD and OCNFDE solutions and between the CCNFD and OCNFDE/EDI solutions, and the correlation coefficients (CC) between the OCNFDE and OCNFDE/EDI solutions. RMSE and CC are, respectively, obtained by means of the following formulas:

$$\mathrm{RMSE}\big(\vartheta_r^n\big) = \sqrt{\frac{1}{M-1}\sum_{i=1}^{M-1}\big|\vartheta_i^n - \vartheta_{ri}^n\big|^2}, \quad r = d \text{ or EDI}, n = 1, 2, \ldots, 250;$$
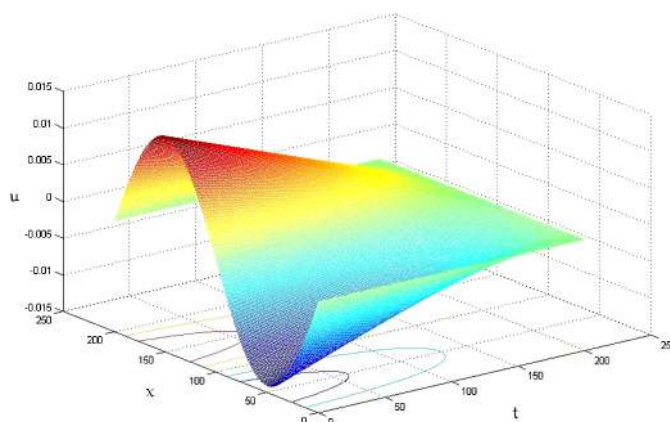
Figure 4 The OCNFDE solutions when $0 \leq t \leq 2.5$ and $0 \leq x \leq 2.5$
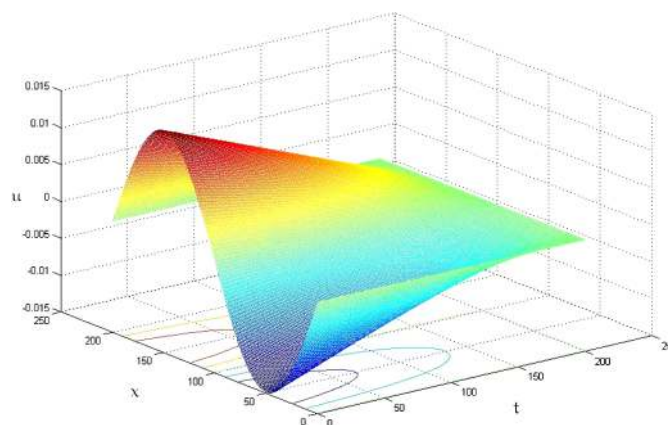
Figure 5 The OCNFDE/DEI solutions when $0 \leq t \leq 2.5$ and $0 \leq x \leq 2.5$

Table 2 Comparisons of CC, RMSE, and CPU time of the OCNFDE and OCNFDE/EDI solutions

n	$CC(n) \times 10^{-4}$	OCNFDE scheme		OCNFDE/EDI scheme	
		RMSE	CPU time	RMSE	CPU time
$n = 150$	1.6214	0.00032	2.88 seconds	0.00046	1.68 seconds
$n = 200$	1.6279	0.00042	3.84 seconds	0.00063	2.24 seconds
$n = 250$	1.6472	0.00068	4.80 seconds	0.00087	2.80 seconds

$$CC(n) = \frac{\sum_{i=1}^{250}(\vartheta_{di}^{n} - \bar{\vartheta}_{di}^{n})(\vartheta_{\text{EDI}i}^{n} - \bar{\vartheta}_{\text{EDI}i}^{n})}{\sqrt{\sum_{i=1}^{250}(\vartheta_{di}^{n} - \bar{\vartheta}_{di}^{n})^2 \sum_{i=1}^{250}(\vartheta_{\text{EDI}i}^{n} - \bar{\vartheta}_{\text{EDI}i}^{n})^2}}, \quad n = 1, 2, \ldots, 250,$$

where $\bar{\vartheta}_{rj}^{n}$ ($r = d$ or EDI) are the expected values of ϑ_{rj}^{n}, respectively. Table 2 shows that the CPU time between the OCNFDE and OCNFDE/DEI methods, RMSEs between the CCNFD and OCNFDE solutions and between the CCNFD and OCNFDE/EDI solutions, and CCs between the OCNFDE and OCNFDE/EDI solutions at $t = 1.5, 2.0,$ and 2.5, respectively.

Table 2 shows that the CPU time of the OCNFDE/EDI model is less than that of the OCNFDE one due to adopting EDI method, but it is reasonable that RMSEs of the OCNFDE/EDI model is slightly larger than those of the OCNFDE model thanks to the nonlinear terms **G** being approximated with EDI. It shows that the OCNFDE/EDI methd is better than the OCNFDE method.

6 Conclusions

In this paper, we have established the OCNFDE model including very few unknowns but holding fully second-order accuracy for the FOPTSGEs (1)–(3), discussed the existence, stabilization, and convergence for the OCNFDE solutions. We have also utilized two numerical examples to verify the effectiveness and feasibility of the OCNFDE and OCNFDE/EDI models (but the OCNFDE/EDI method is better than the OCNFDE method) and to validate that the numerical calculated conclusions coincide with the theoretical results. Specially, the OCNFDE model is far superior to the CCNFD model, since the OCNFDE model can immensely spare the CPU consumption time and reduce the unknowns in comparison with the CCNFD model. Moreover, the CCNFD and OCNFDE models are denoted by the matrix forms and the stability and error estimates for the OCNFDE so-

lutions are proved by using the matrix analysis, so that the theoretical analysis and the numerical computations become more concise and convenient. In addition, as the OC-NFDE model for the FOPTSGEs (1)–(3) is first established, it is an improvement of other existing reduced-order models mentioned in Sect. 1.

Although we only have studied the order reduction of the CCNFD model for the FOPTS-GEs (1)–(3), because the CCNFD model can solve FOPTSGEs in a two- and three-dimensional unbounded domain (see, e.g., [3]), the OCNFDE model can easily and effectively be applied to reduce the order for the FOPTSGEs (1)–(3) in two- and three-dimensional domains.

Author details
[1] School of Science, Beijing Technology and Business University, Beijing, China. [2] School of Mathematics and Physics, North China Electric Power University, Beijing, China.

Publisher's Note
Springer Nature remains neutral with regard to jurisdictional claims in published maps and institutional affiliations.

References

1. Dehghan, M., Manafian, J., Saadatmandi, A.: Solving nonlinear fractional partial differential equations using the homotopy analysis method. Numer. Methods Partial Differ. Equ. **26**(2), 448–479 (2010)
2. Kilbas, A.A., Srivastava, H.M., Trujillo, J.J.: Theory and Applications of Fractional Differential Equations. Elsevier, Amsterdam (2006)
3. Liu, F., Zhuang, P., Liu, Q.X.: Numerical Methods of Fractional Partial Differential Equations and Their Applications. Science Press, Beijing (2015) (in Chinese)
4. Cao, Y.H., Luo, Z.D.: A reduced-order extrapolating Crank–Nicolson finite difference scheme for the Riesz space fractional order equations with a nonlinear source function and delay. J. Nonlinear Sci. Appl. **11**, 672–682 (2018)
5. Elsaid, A., Hammad, D.: A reliable treatment of homotopy perturbation method for the sine-Gordon equation of arbitrary (fractional) order. J. Fract. Calc. Appl. **2**(1), 1–8 (2012)
6. Yousef, A.M., Rida, S.Z., Ibrahim, H.R.: Approximate solution of fractional-order nonlinear sine-Gordon equation. Elixir Appl. Math. **82**, 32549–32553 (2015)
7. Macías-Díaz, J.E.: Numerical study of the process of nonlinear supratransmission in Riesz space-fractional sine-Gordon equations. Commun. Nonlinear Sci. Numer. Simul. **46**(1), 89–102 (2017)
8. Zhou, Y.J., Luo, Z.D.: A Crank–Nicolson finite difference scheme for the Riesz space fractional order parabolic type sine-Gordon equation. Adv. Differ. Equ. **2018**, 137, 1–7 (2018)
9. Sirovich, L.: Turbulence and the dynamics of coherent structures: parts I–III. Q. Appl. Math. **45**(3), 561–590 (1987)
10. Holmes, P., Lumley, J.L., Berkooz, G.: Turbulence, Coherent Structures, Dynamical Systems and Symmetry. Cambridge University Press, Cambridge (1996)
11. Cazemier, W., Verstappen, R.W.C.P., Veldman, A.E.P.: Proper orthogonal decomposition and low-dimensional models for driven cavity flows. Phys. Fluids **10**(7), 1685–1699 (1998)
12. Ly, H.V., Tran, H.T.: Proper orthogonal decomposition for flow calculations and optimal control in a horizontal CVD reactor. Q. Appl. Math. **60**(4), 631–656 (1989)
13. Fukunaga, K.: Introduction to Statistical Recognition. Academic Press, New York (1990)
14. Jolliffe, I.T.: Principal Component Analysis. Springer, Berlin (2002)
15. Selten, F.M.: Baroclinic empirical orthogonal functions as basis functions in an atmospheric model. J. Atmos. Sci. **54**(16), 2099–2114 (1997)

16. Kunisch, K., Volkwein, S.: Galerkin proper orthogonal decomposition methods for parabolic problems. Numer. Math. **90**(1), 117–148 (2001)
17. Kunisch, K., Volkwein, S.: Galerkin proper orthogonal decomposition methods for a general equation in fluid dynamics. SIAM J. Numer. Anal. **40**(2), 492–515 (2002)
18. Luo, Z.D., Chen, J., Navon, I.M., Yang, X.Z.: Mixed finite element formulation and error estimates based on proper orthogonal decomposition for the non-stationary Navier–Stokes equations. SIAM J. Numer. Anal. **47**(1), 1–19 (2008)
19. Luo, Z.D., Li, H., Zhou, Y.J., Xie, Z.H.: A reduced finite element formulation based on POD method for two-dimensional solute transport problems. J. Math. Anal. Appl. **385**(1), 371–383 (2012)
20. Luo, Z.D., Yang, X.Z., Zhou, Y.J.: A reduced finite difference scheme based on singular value decomposition and proper orthogonal decomposition for Burgers equation. J. Comput. Appl. Math. **229**(1), 97–107 (2009)
21. Sun, P., Luo, Z.D., Zhou, Y.J.: Some reduced finite difference schemes based on a proper orthogonal decomposition technique for parabolic equations. Appl. Numer. Math. **60**(1–2), 154–164 (2010)
22. Luo, Z.D., Xie, Z.H., Shang, Y.Q., Chen, J.: A reduced finite volume element formulation and numerical simulations based on POD for parabolic problems. J. Comput. Appl. Math. **235**(8), 2098–2111 (2011)
23. Luo, Z.D., Li, H., Zhou, Y.J., Huang, X.M.: A reduced FVE formulation based on POD method and error analysis for two-dimensional viscoelastic problem. J. Math. Anal. Appl. **385**(1), 310–321 (2012)
24. Benner, P., Cohen, A., Ohlberger, M., Willcox, A.K.: Model Reduction and Approximation: Theory and Algorithm. Computational Science & Engineering. SIAM, Philadelphia (2017)
25. Hesthaven, J.S., Rozza, G., Stamm, B.: Certified Reduced Basis Methods for Parametrized Partial Differential Equations. Springer, Berlin (2016)
26. Quarteroni, A., Manzoni, A., Negri, F.: Reduced Basis Methods for Partial Differential Equations. Springer, Berlin (2016)
27. Dehghan, M., Abbaszadeh, M.: An upwind local radial basis functions-differential quadrature (RBF-DQ) method with proper orthogonal decomposition (POD) approach for solving compressible Euler equation. Eng. Anal. Bound. Elem. **92**, 244–256 (2018)
28. Dehghan, M., Abbaszadeh, M.: A reduced proper orthogonal decomposition (POD) element free Galerkin (POD-EFG) method to simulate two-dimensional solute transport problems and error estimate. Appl. Numer. Math. **126**, 92–112 (2018)
29. Dehghan, M., Abbaszadeh, M.: A combination of proper orthogonal decomposition-discrete empirical interpolation method (POD-DEIM) and meshless local RBF-DQ approach for prevention of groundwater contamination. Comput. Math. Appl. **75**(4), 1390–1412 (2018)
30. Dehghan, M., Abbaszadeh, M.: The use of proper orthogonal decomposition (POD) meshless RBF-FD technique to simulate the shallow water equations. J. Comput. Phys. **351**, 478–510 (2017)
31. Luo, Z.D., Li, H., Sun, P., Gao, J.Q.: A reduced-order finite difference extrapolation algorithm based on POD technique for the non-stationary Navier–Stokes equations. Appl. Math. Model. **37**(7), 5464–5473 (2013)
32. Luo, Z.D., Gao, J.Q.: A POD-based reduced-order finite difference time-domain extrapolating scheme for the 2D Maxwell equations in a lossy medium. J. Math. Anal. Appl. **444**, 433–451 (2016)
33. Xia, H., Luo, Z.D.: An optimized finite difference iterative scheme based on POD technique for the 2D viscoelastic wave equation. Appl. Math. Mech. **38**(12), 1721–1732 (2017)
34. Xia, H., Luo, Z.D.: A POD-based optimized finite difference CN extrapolated implicit scheme for the 2D viscoelastic wave equation. Math. Methods Appl. Sci. **40**(15), 6880–6890 (2017)
35. Liu, S., Fu, Z.T., Liu, S.: Exact solutions to sine-Gordon-type equations. Phys. Lett. A **351**, 59–63 (2006)
36. Luo, Z.D., Chen, G.: Proper Orthogonal Decomposition Methods for Partial Differential Equations. Mathematics in Science and Engineering. Elsevier, Amsterdam (2018). https://www.elsevier.com/books/proper-orthogonal-decomposition-methods-for-partial-differential-equations/luo/978-0-12-816798-4
37. Chung, T.: Computational Fluid Dynamics. Cambridge University Press, Cambridge (2002)
38. Zhang, W.S.: Finite Difference Methods for Partial Differential Equations in Science Computation. Higher Education Press, Beijing (2006)
39. Chaturantabut, S., Sorensen, D.C.: Nonlinear model reduction via discrete empirical interpolation. SIAM J. Sci. Comput. **32**(5), 2737–2764 (2010)